Removal of molybdenum(VI) from aqueous solutions using nano zero-valent iron supported on biochar enhanced by cetyl-trimethyl ammonium bromide: adsorption kinetic, isotherm and mechanism studies

J. J. Lian, Y. G. Huang, B. Chen, S. S. Wang, P. Wang, S. P. Niu and Z. L. Liu

ABSTRACT

A new carbonized pomelo peel biosorbent (MCPP) modified with nanoscale zero-valent iron (NZVI) and cetyl-trimethyl ammonium bromide was prepared and employed for the adsorption of molybdate (Mo(VI)) from aqueous solution. We investigated the effects of various conditions on Mo(VI) adsorption and evaluated the results based on adsorption kinetics models and isotherm equations. The kinetic data fitted to the pseudo-second-order model. The Langmuir model best described the adsorption of Mo(VI) on MCPP. The values of changes in Gibbs free energy, standard enthalpy, and standard entropy revealed that the adsorption process was feasible, spontaneous and endothermal. X-ray diffraction, Fourier transform infrared and X-ray photoelectron spectroscopy measurements suggested that Mo(VI) adsorption occurred via both the reduction and surface adsorption. Thus, biochar, prepared from fruit residue, can be applied to remove Mo(VI) from aqueous solutions. More importantly, our results provide a sustainable approach for Mo(VI) removal from wastewater by means of functional modification.

Key words | adsorption, biochar, molybdenum, nano zero-valent iron, pomelo peel

J. J. Lian
B. Chen (corresponding author)
S. S. Wang
P. Wang
S. P. Niu
Z. L. Liu
College of Energy and Environment,
Anhui University of Technology,
Anhui 243002,
China
E-mail: *greenchenbo@163.com*

Y. G. Huang
School of Environmental Science and Engineering,
Hubei Polytechnic University,
Huangshi 435003,
China

INTRODUCTION

Molybdenum (Mo) is an essential trace element for both plants and animals. It exists in various oxidation states ranging from +2 to +6 in aqueous solution, and molybdate (MoO_4^{2-}) is the most soluble among Mo compounds (Lian *et al.* 2013b). Mo compounds have a relatively low level of toxicity at <5 μg/L (Agarwal *et al.* 2016). However, due to the massive amounts of Mo effluents generated from mining tailings, Mo concentrations ranging from several tens of μg/L to mg/L have detected in water systems (Tu *et al.* 2016). Moreover, incidents of Mo pollution have been reported in Brenda Mines in British Columbia, Canada; the San Joaquin Valley, USA; and Wujintang Reservoir, China (Lian *et al.* 2013a; Halmi *et al.* 2014). As the maximum contaminant level for Mo in the drinking water reached 0.07 mg/L according to People's Republic of China(PRC), the lack of feasible methods for Mo removal from aqueous solutions has become a growing concern for the sustainable use of natural resources.

Adsorption has gained broad interest for removal of pollutants because it is an efficient and economically feasible process for purification. Biosorption processes are relatively easy to operate and offer several advantages including low cost, operation over a wide range of conditions and possible reuse of biosorbents. As a result, many researchers have investigated low-cost, biodegradable substitutes made from natural resources to remove toxic ions from wastewater (Namasivayam & Sureshkumar 2009; Lou *et al.* 2015).

Biochar is a carbon-rich solid produced by thermal decomposition of biomass under a limited oxygen supply at ≤700°C. Many studies have focused on applying biochar as a biosorbent in wastewater treatment for its large specific surface area, highly porous structure, and strong redox reactivity (Shan *et al.* 2012; Yao *et al.* 2015). However, biochar utilized in these studies was negatively charged, so functionalizing biochar particles with positively charged metal cations could be an efficient way for oxoanion removal from aqueous solutions.

Maintaining the chemical stability of positively charged biochar particles against dissolution in acidic medium and oxidization is challenging. Metal-cation-loaded biochar

doi: 10.2166/wst.2018.258

particles are coated with polymers to overcome these problems. Pomelo is abundant as a biological resource worldwide, particularly in a big agricultural country such as China. Moreover, pomelo has more peel and segment membrane than most other citrus fruits, generating a significant quantity of pomelo waste. As the pomelo residue, pomelo peel (PP) is mainly composed of cellulose, hemicellulose, and lignin. Large amounts of PP are disposed of after consumption, resulting in the wastage of resources and land. However, modified PP using different activation methods to remove Reactive Blue 114 dye and malachite green dye from wastewater have been studied in recent years (Argun *et al.* 2014; Bello *et al.* 2015). We hypothesized that the adsorption of post-transition metals by modified carbonized pomelo peel (MCPP) can offer efficient treatment of effluent wastewater. However, such information is unknown to date.

In this study, the adsorption of Mo(VI) from aqueous solution on PP biochar modified by nano zero-valent iron (NZVI) and cationic surfactant cetyl-trimethyl ammonium bromide (CTAB) was investigated. Adsorption dynamics, equilibrium studies, and the effects of pH and temperature were particularly investigated. Further information about the binding mechanism was also obtained.

MATERIAL AND METHODS

Materials

All chemicals used such as hydrochloric acid, sodium hydroxide, and CTAB were of analytical reagent grade and purchased from Sinopharm Chemical Reagent Co., Ltd (China). Ammonium heptamolybdate ($(NH_4)_6Mo_7O_{24}{\cdot}4H_2O$) was employed to prepare a stock solution containing 1,000 mg/L Mo which was further diluted with deionized water as desired. All reagents were of analytical grade and were used without further purification.

Preparation of modified PP

PP was collected from the local market as solid waste. It was washed with distilled water several times to remove the dirt particles, and then milled, rinsed, dried, and pulverized to a particle size <2.0 mm for testing. Carbonized pomelo peel (CPP) was prepared by pyrolysis under N_2 at 500 °C for 1 h in a tube furnace. NZVI was prepared by Fe^{2+} solution with the traditional synthetic method. Five grams of CPP was mixed with 100 mL 0.2 M $FeSO_4$ aqueous solution and stirred for 1 h under N_2. Then 100 mL 0.2 M KBH_4 was slowly added to this solution and stirred at 120 rpm for 30 min, and the jet-black nanoparticle aggregates were formed. Subsequently, 100 mL 0.02 M CTAB solution was added to this solution and stirred for another 1 h. The resulting modified CPP (MCPP) was filtered and washed successively with distilled water and absolute ethyl alcohol solution to remove unreacted substances. Finally, the prepared MCPP was dried at 60 °C in a vacuum oven for 12 h, and stored in a sealed polyethylene container for further Mo adsorption studies.

Batch experiments for Mo(VI) adsorption

MCPP (1 g/L) was added to 100 mL Mo(VI) solutions (0–100 mg/L) at pH 4 ± 0.3 by shaking the mixture at 278, 298, and 318 K, respectively, to obtain adsorption isotherms. NaCl (0.1 M) was used as a background electrolyte to maintain a constant ionic strength for comparison between different experiments. Adsorption kinetics for Mo(VI) was investigated by adding MCPP (1 g/L) to 100 mL Mo(VI) solutions (20 mg/L) with 0.1 M NaCl solution at pH 4 ± 0.3. After the adsorption equilibrium was reached, the suspensions were filtered through 0.45 μm pore-size filters, and the residual molybdate was analyzed. All adsorption experiments were performed in triplicate.

The initial pH of the mineral suspensions containing Mo(VI) was adjusted to the range of 1.0–10.0 by adding 1 M HCl or 1 M NaOH while maintaining <2% change in total volume. The pH value of the solution was measured by a S-3C model pH meter. The pH of point of zero charge (pHpzc) of the material was tested by the mass titration method; that is, the pH of the system approaches $pH_\infty = (pK_1 + pK_2)$ pzc/2 under the limiting conditions of 'infinite' mass/volume ratio (Noh & Schwarz 1989). Percentage adsorption (%A) of Mo was calculated according to Equation (1):

$$\%A = \frac{(C_i - C_e)}{C_i} \times 100 \quad (1)$$

where C_i is the initial concentration of Mo and C_e stands for the equilibrium concentration measured after adsorption on the MCPP.

Adsorbent characterization

The structure and surface characteristics of adsorbents were measured using scanning electron microscopy (SEM; FEI Quanta 200). The surface elemental analysis was also conducted simultaneously using energy dispersive X-ray

spectroscopy (EDS) along with SEM (FEI Quanta 200). The specific surface area was measured by Brunauer–Emmett–Teller method using a Micromeritics Tristar 3020. Powder X-ray diffraction (XRD) patterns at 2θ angles from 10° to 80° were recorded at an interval of 0.33° on an UItima IV diffractometer using Cu radiation (40 kV, 40 mA). Fourier transform infrared (FTIR) spectra were recorded on a Nicolet 6700 FTIR spectrophotometer. X-ray photoelectron spectroscopy (XPS) analysis was conducted by an Escalab 250Xi with the monochromatic Al Kα X-ray radiation. The concentrations of molybdate were measured using a PE AA700 model atomic absorption spectrophotometer.

RESULTS AND DISCUSSION

Characteristics of adsorbent

The ordered structures of CPP, MCPP, and MCPP-Mo were identified with XRD analysis, shown in Figure 1. The results revealed the diffraction peaks appeared at 25°on CPP, which is the characteristic peak of graphite crystal. The characteristic peaks at 44.67° confirmed the presence of Fe^0 on MCPP in comparison to the peaks of the standard materials. The peaks at 32.6° and 35.87° on MCPP-Mo belonged to maghemite magnetite (Fe_3O_4) (Fu *et al.* 2017), whereas the peaks at 26.3°, 54.7° and 59.8° on MCPP-Mo demonstrated the existence of MoO_2 (Sun *et al.* 2011). From the indexed XRD pattern (JCPDS No. 50-1619), the strongest intense peaks corresponding to 2θ value of 19.5°, 20.3°, 21.7°, and 22.9° confirmed the existence of $Fe_2(MoO_4)_3$ on MCPP-Mo. The results indicated that Mo(VI) was partially adsorbed on MCPP, and the unadsorbed species were reduced to lower valence state by NZVI.

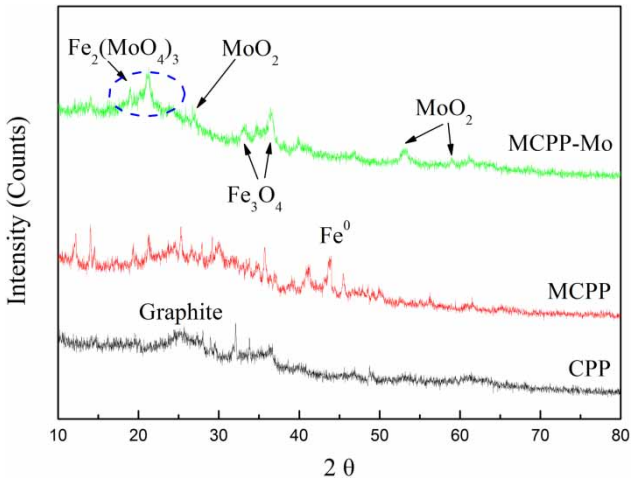

Figure 1 | XRD spectra of the CPP, MCPP, and MCPP-Mo.

A scanning electron microscope equipped with EDS analysis was used to find out the change in morphology before and after modification, as shown in Figure 2. In general, the morphology of the original biochar (CPP) was porous with a rough surface probably because of the intrinsic nature of the PP (Figure 2(a)), and MCPP had a relatively smaller pore structure for the injection of NZVI and CTAB (Figure 2(b)). In EDS analysis, C, O, and K appeared as the major elements in CPP since they are characteristic for biological carbon. However, the atomic ratio of Ca, K, and Mg in CPP decreased from 1.68%, 3.61%, and 0.74% to 0.08%, 0, and 0.07% after modification, respectively. The new peaks (Fe) appeared in MCPP, which indicated that Ca, K, and Mg were partly replaced by Fe in the modification process. The atomic ratio of C, O, Fe, and S in MCPP was found to be 73.66%, 24.16%, 1.38%, and 0.58%, respectively. Furthermore, the specific surface areas of CPP and MCPP were determined to be 98.74 m^2/g and 31.20 m^2/g, respectively.

The effect of pH on the adsorption behavior of MCPP

A solution of 20 mg/L Mo(VI) and 1 g/L of adsorbent were used to examine the pH effect. The results (Figure 3) show that the maximum Mo adsorption occurs in pH range 2.0–4.0. The maximum removal can be due to the change of Mo(VI) to other species and the surface protonation of the sorbent. The pHzpc of the MCPP is 5.20. However, the speciation of molybdate anions are anionic polynuclear hydrolyzed species in pH range 2.0–4.6: $Mo_7O_{21}(OH)_3^{3-}$, $Mo_7O_{22}(OH)_2^{4-}$, $Mo_7O_{23}(OH)^{5-}$, $Mo_7O_{24}^{6-}$ (Xiong *et al.* 2011). Consequently, the adsorbent surface is positively charged below the pHzpc; thus anion adsorption occurs. The lower removal rate at pH < 2.0 may be attributed to the higher concentration of Cl^-, which competes with molybdate anions for interaction with active adsorbent sites (Elwakeel *et al.* 2009). The decrease in the removal at pH > 6.0 is due to the decrease in surface protonation and competition of OH^-. When the pH increased to 9.0, the percentage of adsorption decreased rapidly toward a negligible level of removal efficiency by the end of the test (<30%). Other studies reported similar observations (Lian *et al.* 2013a).

Adsorption kinetics of Mo(VI) adsorption on MCPP

The adsorption of Mo(VI) on MCPP was investigated as a function of contact time, at different initial Mo(VI)

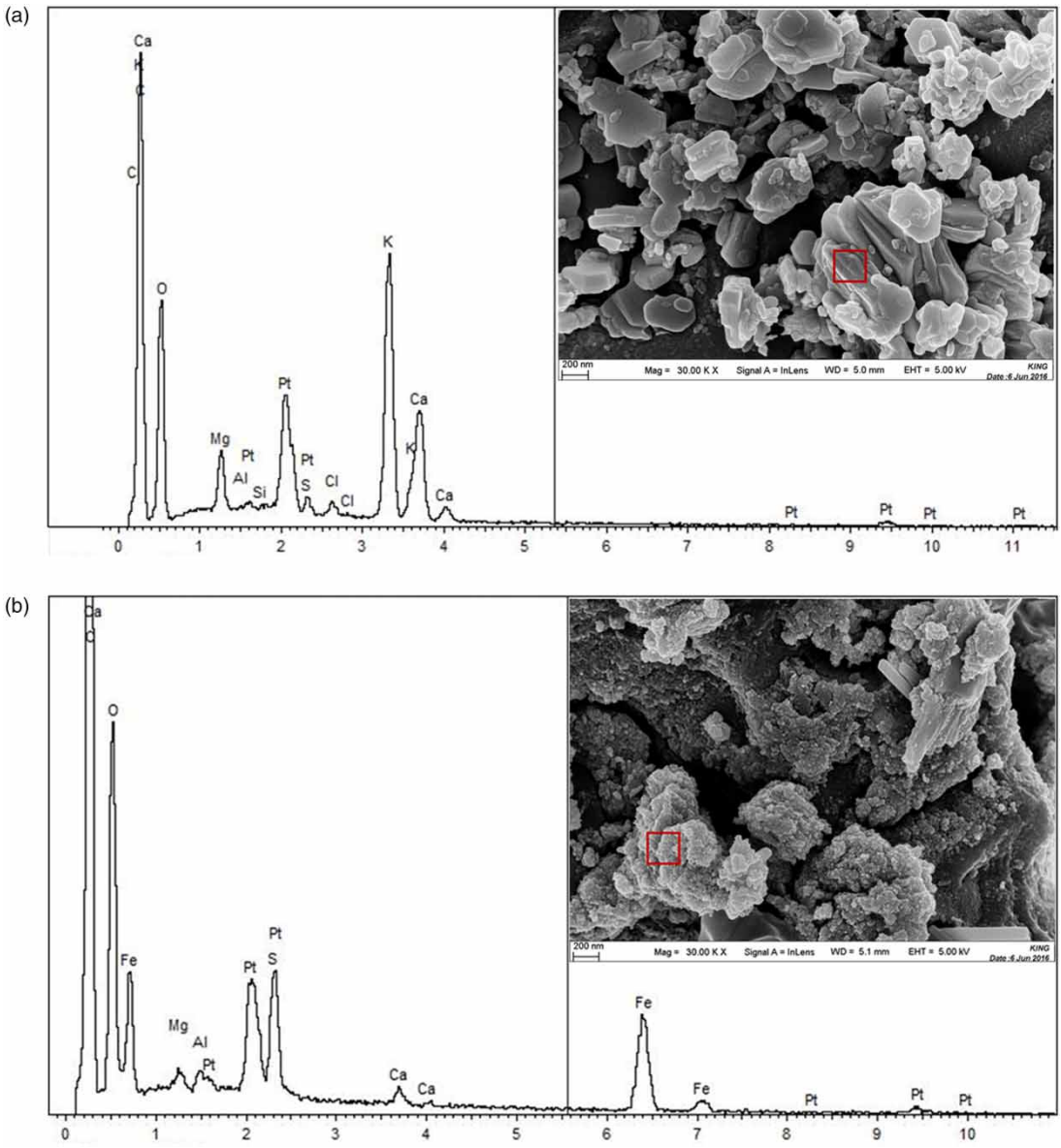

Figure 2 | SEM-EDS images of (a) CPP and (b) MCPP.

concentrations, in the range of 0–180 min at 298 K. Four common kinetic models, the pseudo-first-order model, pseudo-second-order model, intra-particle diffusion model, and Elovich mass transfer model, were employed to describe the adsorption process of Mo(VI) on MCPP. The expression formulas and the correlative parameters of these kinetic models with the correlation coefficients (R^2) are presented in Table 1.

The kinetic data showed a rapid initial uptake followed by a smooth increase, with equilibrium reached in less than 160 min (Figure 4). Moreover, it can be observed that the correlation coefficient for the second-order kinetic equation was greater than 0.99. The calculated q_e values also agree well with the experimental data ($q_{exp} = 19.91$ mg/g). These results indicate that adsorption of Mo(VI) onto the MCPP is best represented with the pseudo-second-order kinetic model based on the assumption that the rate-limiting step may be chemisorption involving valence forces through sharing or exchange of electrons between adsorbate and adsorbent (Shan *et al.* 2016).

Adsorption isotherms on MCPP

The adsorption isotherms demonstrate the specific relation between the concentration of adsorbate and its

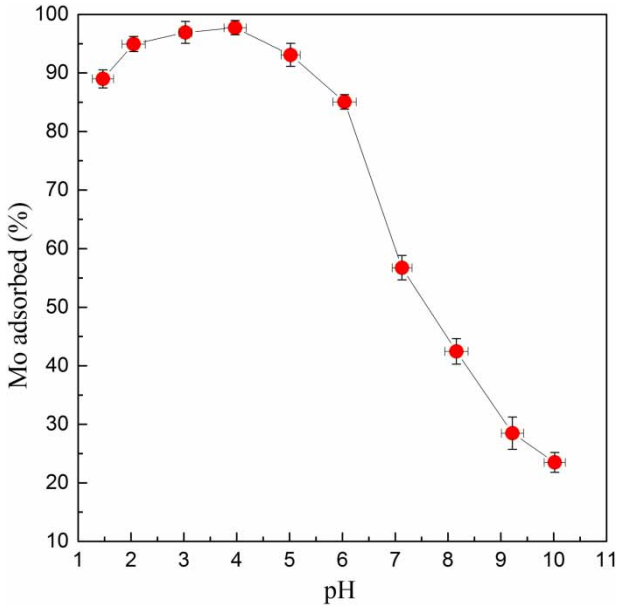

Figure 3 | Effects of varying equilibrium pH values on Mo(VI) adsorption. Conditions: solid/liquid = 1 g/L, T = 298 K, initial Mo concentration = 20 mg/L.

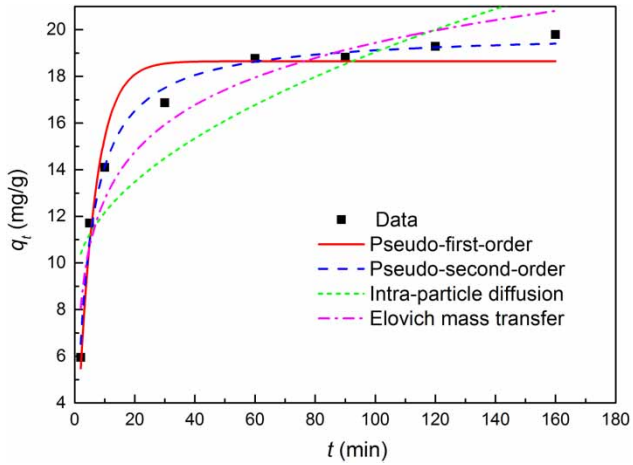

Figure 4 | Adsorption kinetic data and modeling for Mo(VI) on MCPP. Symbols are experimental data, and lines are model results. Solid/liquid = 1 g/L, temperature = 298 K, pH = 4.0.

degree of accumulation onto the adsorbent surface at a constant temperature. Several isotherm models have been used to fit the experimental data and evaluate the isotherm performance for Mo(VI) adsorption. These isotherm models include Langmuir isotherm, Freundlich isotherm, Temkin isotherm and Dubinin–Radushkevich isotherm, and the corresponding equations were expressed in our previous work (Lian *et al.* 2013a). The adsorption plots and the fitting model parameters with R^2 for the different models are separately shown in Figure 5 and Table 2.

Table 1 | Comparison of the four kinetic models for Mo(VI) adsorption on MCPP at 298 K

Kinetic models	Expression formula	Parameters	298 K
Pseudo-first-order	$\ln(q_e - q_t) = \ln q_e - k_1 t$	q_e (mg/g)	18.65
		k_1 (1/min)	0.17
		R^2	0.95
Pseudo-second-order	$\frac{t}{q_t} = \frac{1}{k_2 q_e^2} + \frac{t}{q_e}$	q_e (mg/g)	19.90
		k_2 (mg/(g·min))	0.01
		R^2	0.99
Intra-particle diffusion	$q_t = k_{dif} t^{1/2} + d$	k_{dif} (mg/g·min$^{1/2}$)	1.01
		D	8.98
		R^2	0.73
Elovich mass transfer	$q_t = \beta \ln(\alpha\beta) + \beta \ln(t)$	α (mg/(g·min))	2.74
		β (g/mg)	2.91
		R^2	0.93

It is evident that the Langmuir isotherm shows a better fit to the adsorption data for MCPP in terms of coefficient of determination ($R^2 > 0.98$). It may be due to the homogeneous distribution of active sites on the adsorbent surface. A comparison of Mo(VI) adsorption capacity of some adsorbents based on the values of Q_0 (Table 3) is comparable to the results obtained in previous studies. It was found that MCPP had a higher adsorption capacity (37.60–48.54 mg/g) in comparison to the reported adsorbents. Therefore, considering the inexpensive PP solid waste, MCPP can be used as an alternative material to recover molybdenum ions from solution.

An essential characteristic of the Langmuir isotherm can be expressed by a dimensionless separation factor (R_L) which was shown in our previous work (Lian *et al.* 2013a). The effect of equilibrium parameter R_L values in the range of $0 < R_L < 1$ at different temperatures further indicated that the biosorbent was favorable for Mo(VI) removal from aqueous solution (see Table 2). However, according to the analysis of the Dubinin–Radushkevich model, the E value was between 1.0 and 8.0 kJ/mol at different temperatures, indicating that the adsorption behavior of Mo(VI) on MCPP could be due to the weak interaction of Mo(VI) with this adsorbent (Bayramoğlu & Arıca 2009).

From the Temkin isotherms, typical bonding energy for the ion exchange mechanism varies in the range of 8–16 kJ/mol while the physisorption process was reported to have adsorption energies less than −40 kJ/mol (Helfferich 1962). The value of b_T (0.50–0.52 kJ/mol) obtained in this study indicated that the adsorption process involves both the chemisorption and physisorption.

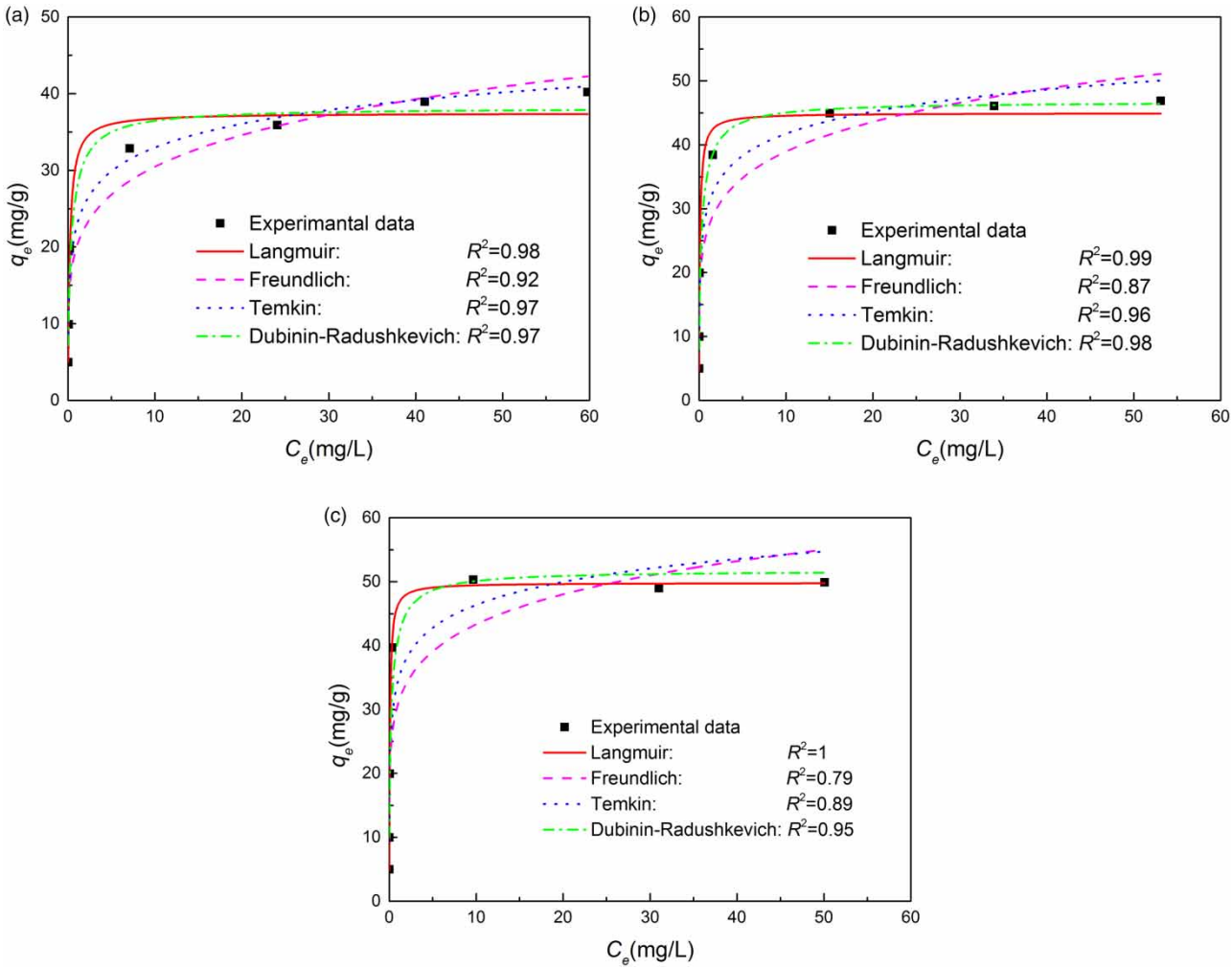

Figure 5 | Adsorption isotherms data and modeling for Mo(VI) on MCPP. Symbols are experimental data, and lines are model results. Solid/liquid = 1 g/L, shaking time = 24 h, temperature = 278 K (a), 298 K (b), 318 K (c), pH = 4.0.

Table 2 | Isotherm model parameters for Mo(VI) adsorption to MCPP at three temperatures

Isotherm models	Expression formula	Parameters	278 K	298 K	318 K
Langmuir	$\frac{C_e}{q_e}=\frac{C_e}{Q_0}+\frac{1}{Q_0 b}$	Q_0 (mg/g)	37.60	44.05	48.54
		b (L/mg)	4.93	11.35	14.71
		$R_L \times 10^2$	0.20–3.90	0.09–1.73	0.07–1.34
		R^2	0.98	0.99	1
Freundlich	$\ln q_e=\frac{1}{n}\ln C_e+\ln k_F$	k_F ($mg^{1-n}\cdot L^n$ /g)	17.56	23.38	26.94
		n	4.23	4.33	4.44
		R^2	0.92	0.87	0.79
Temkin	$q_e=\frac{RT}{b_T}\ln A+\frac{RT}{b_T}\ln C_e$	A (L/g)	0.16	0.44	0.77
		b_T (kJ/mol)	0.52	0.5	0.51
		R^2	0.97	0.96	0.89
Dubinin–Radushkevich	$\ln Q_e=\ln Q_m-\beta\varepsilon^2$	Q_m (mg/g)	39.41	48.77	56.47
		β (mol^2/kJ)	0.23	0.18	0.17
		E (kJ/mol)	1.46	2	1.73
		R^2	0.97	0.98	0.95

Table 3 | Comparison between the adsorption of Mo(VI) by MCPP and other adsorbents reported in the literature

Adsorbents	Adsorption capacity (mg/g)	References
Nano-magnetic $CuFe_2O_4$	30.58	Tu *et al.* (2014)
NaOCl-oxidized multiwalled carbon nanotubes	22.73	Chen & Lu (2014)
Di-(2-ethylhexyl) phosphoric acid	25.84	Fu *et al.* (2017)
Maghemite nanoparticles	33.4	Afkhami & Asl (2009)
Desulfurization steel slag	4.38	Lian *et al.* (2013a)
Modified pomelo peel	48.54	This study

Thermodynamics of Mo(VI) adsorption on MCPP

The effect of temperature is a major influencing factor in the adsorption process. The Mo(VI) adsorption of MCPP was monitored at three different temperatures (278, 298, and 318 K) under optimized conditions by adapting the Khan and Singh method (Khan & Singh 1987). Thermodynamic parameters ΔG° (change in Gibbs free energy) ΔH° (change in standard enthalpy) and ΔS° (change in standard entropy) are presented in Table 4. The values of ΔH° were positive in the process of Mo(VI) absorbed on MCPP, suggesting that the adsorption reaction was endothermic. The positive value of ΔS° shows the increased randomness at the solid/solution interface during the adsorption of Mo(VI) on MCPP. The negative values of ΔG° indicated that the adsorption process was spontaneous in nature. The ΔG° values obtained in this study for Mo(VI) were less than -10 kJ/mol, suggesting that the physical adsorption played a role in the adsorption process. The results are in agreement with the Dubinin–Radushkevich isotherm model.

Adsorption mechanism of Mo(VI) on MCPP

The sorption pattern of metals onto materials is attributable to the active groups and bonds present on sorption materials. Therefore, FTIR spectroscopy was employed to identify the functional groups in the native sorbent (CPP), modified sorbent (MCPP), and Mo-loaded sorbent (MCPP-Mo). Figure 6 shows the spectra of CPP and MCPP with differences in the impregnation of modifiers. Compared with the spectrum of CPP, the decrease in the intensity of the absorption peak at 1,428 cm^{-1} as well as the peak around 1,162 cm^{-1} can be observed in the spectrum of MCPP. The two peaks correspond to C-O symmetric stretching and C-N stretching, respectively (Lou *et al.* 2015). The absorption peak around 3,426 cm^{-1} can be assigned to O-H and -NH stretching (Lou *et al.* 2015). The peaks around 2,922 cm^{-1} correspond to the CH_2 asymmetric stretching vibration. The peak at 1,624 cm^{-1} presented in MCPP is asymmetric stretching vibrations of ionic carboxylic groups ($-COO^-$) (Iqbal *et al.* 2009). In addition, the peaks around 616 cm^{-1} are a common feature of different oxides such as Fe, Al, and Mg (Navarro *et al.* 2010). These results imply that CTAB and NZVI have been coated on the surface of MCPP.

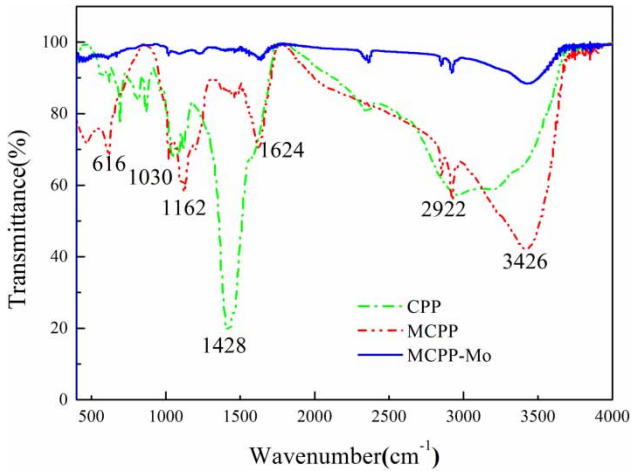

Figure 6 | FTIR spectra of CPP, MCPP, and MCPP-Mo.

Compared with the spectrum of MCPP, the decrease in the intensity of the adsorption peaks around 3,426 cm^{-1} can be observed in the spectrum of MCPP-Mo. Moreover, the presence of broad and weak overtone bands in the region of 1,100–1,800 cm^{-1} might be due to polymeric M_xO_y species (M: V, Mo, and W) (Busca *et al.* 1986). The modification of the band at 1,030 cm^{-1}, which can be assigned to hydroxyl vibrations of iron oxyhydroxides (Namduri & Nasrazadani 2008), indicates that M=O stretching of coordinatively unsaturated surface Mo^{n+} ions may be involved in coordination with Fe ions (Mauge *et al.* 1988). The peaks around 616 cm^{-1} disappeared in MCPP-Mo, indicating an

Table 4 | Thermodynamic parameters for the adsorption of Mo(VI) on MCPP

Temperature (K)	ΔG° (kJ/mol)	ΔH° (kJ/mol)	ΔS° (kJ/(mol·K))	R^2
278	−12.08	25.05	0.13	0.95
298	−15.41			
318	−17.38			

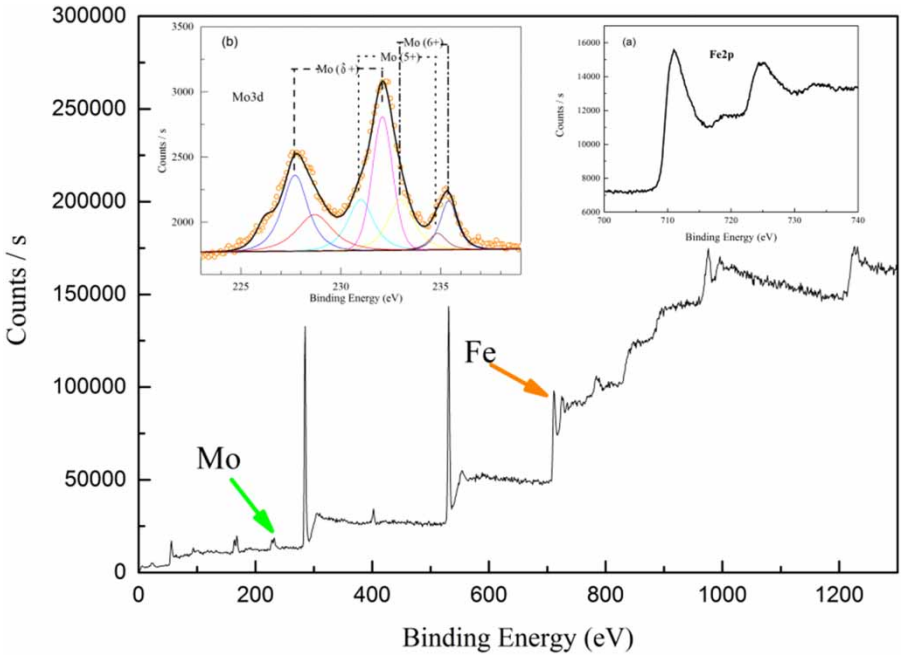

Figure 7 | XPS spectra of the MCPP after Mo(VI) adsorption.

interaction between metallic oxides and Mo(VI) for the impregnation of Mo(VI) ions, which is also verified by the XRD results. These results indicate that diverse interactions exist between MCPP and Mo(VI) for the impregnation of Mo(VI) ions that are in accordance with the previous literature (Pramanik *et al.* 2016).

XPS analysis was performed for further evidence of the adsorption mechanism inferred by the FTIR analysis. As seen from Figure 7, several peaks at binding energies from 0 to 1,300 eV were observed. High-resolution XPS scans have been carried out over the binding energies of interest for different metallic elements to determine the oxide composition. Typical binding energy bands of the chemical states in Fe and Mo are indicated in Figure 7(a) and 7(b). As can be seen from the XPS spectra of Fe (Figure 7(a)), all present peaks at 723.0 eV (Fe $2p_{1/2}$) and 709.0 eV (Fe $2p_{3/2}$) corresponded to Fe_3O_4. Similarly, a small elevation can be observed at 717.0 eV that is characteristic for Fe^{3+} (iron oxide Fe_2O_3), which is grown during deposition or formed in air by oxidation, while the peak at 714.0 eV represents Fe^{2+} (FeO) (Du *et al.* 2006).

The identification of the Mo oxidation state in different compounds and following reduction treatments were monitored throughout the Mo ($3d_{3/2}$, $3d_{5/2}$) spin-orbit components. The binding energies of different oxidation states of Mo are 235.8 and 232.6 eV for MoO_3, 234.9 and 231.7 eV for Mo_2O_5, and 232.3 and 229.1 eV for MoO_2 (Yavuz *et al.* 2015). Also, two species with $Mo3d_{5/2}$ binding energies of 227.8 and 228.7 eV were identified. Since the binding energies of the two species were intermediate between those assigned to Mo^{4+} (232.3 eV) and Mo^0 (227.8 eV), these species were temporarily denoted as $Mo^{\delta+}$ where $0 < \delta < 4$. It appears that the aqueous molybdate (MoO_4^{2-}) was reduced to (0–5)-valent Mo by zero-valent iron, since it has also been suggested by Huang *et al.* (2012). Therefore, we can conclude that the XPS data is in good agreement with the FTIR and XRD data as well as the literature.

CONCLUSIONS

In this study, MCPP was successfully prepared and employed for Mo(VI) adsorption from aqueous solution. The effects of various conditions for the Mo(VI) adsorption were investigated systematically. The experimental data was well fitted to the pseudo-second-order model as well as the Langmuir isotherm model with maximum monolayer adsorption capacity of 48.54 mg/g at 318 K. Thermodynamic parameters revealed that the nature of adsorption was feasible, spontaneous and endothermic. FTIR, XRD, and XPS studies showed that the sorption of Mo(VI) by MCPP was mainly attributed to both the reduction and surface adsorption. Taking account of the low cost and easy

availability of the raw material, and reasonably high adsorption capacity, MCPP can be potentially used for molybdenum removal from wastewater.

ACKNOWLEDGEMENTS

The authors thank the reviewers and editors for their input. We also acknowledge financial support for this research from the National Natural Science Foundation of China (No. 51709001, No. 41401553), Nature Science Foundation of Anhui Province of China (1708085QD81), and the Youth Foundation of Anhui University of Technology (QZ201520).

REFERENCES

Afkhami, A. & Asl, R. N. 2009 Removal, preconcentration and determination of Mo(VI) from water and wastewater samples using maghemite nanoparticles. *Colloids & Surfaces A: Physicochemical & Engineering Aspects* **346** (1), 52–57.

Agarwal, S., Tyagi, I., Gupta, V. K., Hanifpour, F., Maghsudi, M. & Javadian, H. 2016 Mo (IV) adsorption from nitric acid media by di-(2-ethylhexyl) phosphoric acid (D2EHPA) coated silanized magnetite nanoparticles. *Journal of Molecular Liquids* **218**, 346–353.

Argun, M. E., Güclü, D. & Karatas, M. 2014 Adsorption of Reactive Blue 114 dye by using a new adsorbent: Pomelo peel. *Journal of Industrial and Engineering Chemistry* **20** (3), 1079–1084.

Bayramoğlu, G. & Arıca, M. Y. 2009 Construction a hybrid biosorbent using *Scenedesmus quadricauda* and Ca-alginate for biosorption of Cu(II), Zn(II) and Ni(II): kinetics and equilibrium studies. *Bioresource Technology* **100**, 186–193.

Bello, O. S., Ahmad, M. A. & Semire, B. 2015 Scavenging malachite green dye from aqueous solutions using pomelo (*Citrus grandis*) peels: kinetic, equilibrium and thermodynamic studies. *Desalination and Water Treatment* **56** (2), 521–535.

Busca, G., Centi, G., Marchetti, L. & Trifiro, F. 1986 Chemical and spectroscopic study of the nature of a vanadium oxide monolayer supported on a high-surface-area TiO_2 anatase. *Langmuir* **2** (5), 568–577.

Chen, Y. C. & Lu, C. Y. 2014 Kinetics, thermodynamics and regeneration of molybdenum adsorption in aqueous solutions with NaOCl-oxidized multiwalled carbon nanotubes. *Journal of Industrial & Engineering Chemistry* **20** (4), 2521–2527.

Du, G. H., Liu, Z. L., Xia, X., Chu, Q. & Zhang, S. M. 2006 Characterization and application of Fe_3O_4/SiO_2 nanocomposites. *Journal of Sol-Gel Science and Technology* **39** (3), 285–291.

Elwakeel, K. Z., Atia, A. A. & Donia, A. M. 2009 Removal of Mo (VI) as oxoanions from aqueous solutions using chemically modified magnetic chitosan resins. *Hydrometallurgy* **97**, 21–28.

Fu, R. B., Zhang, X., Xu, Z., Guo, X. P., Bi, D. S. & Zhang, W. 2017 Fast and highly efficient removal of chromium(VI) using humus-supported nanoscale zero-valent iron: influencing factors, kinetics and mechanism. *Separation and Purification Technology* **174**, 362–371.

Halmi, M. I. E., Wasoh, H., Sukor, S., Ahmad, S. A., Yusof, M. T. & Shukor, M. Y. 2014 Bioremoval of molybdenum from aqueous solution. *International Journal of Agriculture and Biology* **16**, 848–850.

Helfferich, F., 1962 *Ion-Exchange*. McGraw-Hill, New York, USA.

Huang, Y. H., Tang, C. & Zeng, H. 2012 Removing molybdate from water using a hybridized zero-valent iron/magnetite/Fe(II) treatment system. *Chemical Engineering Journal* **200–202** (34), 257–263.

Iqbal, M., Saeed, A. & Zafar, S. I. 2009 FTIR spectrophotometry, kinetics and adsorption isotherms modeling, ion exchange, and EDX analysis for understanding the mechanism of Cd^{2+} and Pb^{2+} removal by mango peel waste. *Journal of Hazardous Materials* **164**, 161–171.

Khan, A. A. & Singh, R. 1987 Adsorption thermodynamics of carbofuran on Sn(IV) arsenosilicate in H^+, Na^+ and Ca^{2+} forms. *Colloids & Surfaces* **24** (1), 33–42.

Lian, J. J., Xu, S. G., Chang, N. B., Han, C. W. & Liu, J. W. 2013a Removal of molybdenum(VI) from mine tailing effluents with the aid of loessial soil and slag waste. *Environmental Engineering Science* **30** (5), 213–220.

Lian, J. J., Xu, S. G., Zhang, Y. M. & Han, C. W. 2013b Molybdenum(VI) removal by using constructed wetlands with different filter media and plants. *Water Science & Technology* **67** (8), 1859–1866.

Lou, Z. N., Wang, J., Jin, X. D., Wan, L., Wang, Y., Chen, H., Shan, W. J. & Xiong, Y. 2015 Brown algae based new sorption material for fractional recovery of molybdenum and rhenium from wastewater. *Chemical Engineering Journal* **273**, 231–239.

Mauge, F., Gallas, J. P., Lavalley, J. C., Busca, G., Ramis, G. & Lorenzelli, V. 1988 FT-IR and FT-FIR studies of vanadium, molybdenum and tungsten oxides supported on different carriers. *Microchimica Acta* **95** (1–6), 57–61.

Namasivayam, C. & Sureshkumar, V. M. 2009 Removal and recovery of molybdenumfrom aqueous solutions by adsorption onto surfactant-modified coir pith, alignocellulosic polymer. *Clean Soil Air Water* **37** (1), 60–66.

Namduri, H. & Nasrazadani, S. 2008 Quantative analysis of iron oxides using Fourier transform infrared spectrophotometry. *Corrosion Science* **50** (9), 2493–2497.

Navarro, C., Diaz, M. & Villa-Garcia, M. A. 2010 Physico-chemical characterization of steel slag. Study of its behavior under simulated environmental conditions. *Environmental Science & Technology* **44** (14), 5383–5388.

Noh, J. S. & Schwarz, J. A. 1989 Estimation of the point of zero charge of simple oxides by mass titration. *Journal of Colloid and Interface Science* **130** (1), 157–164.

Pramanik, A., Maiti, S. & Mahanty, S. 2016 Superior lithium storage properties of $Fe_2(MoO_4)_3$/ MWCNT composite with a nanoparticle (0D)-nanorod (1D) hetero-dimensional morphology. *Chemical Engineering Journal* **307**, 239–248.

Shan, W. J., Fang, D. W., Zhao, Z. Y., Shuang, Y., Ning, L. Z., Xing, Z. Q. & Xiong, Y. 2012 Application of orange peel for adsorption separation of molybdenum(VI) from Re-containing industrial effluent. *Biomass and Bioenergy* **37**, 289–297.

Shan, W. J., Shu, Y. N., Chen, H., Zhang, D. Y., Wang, W., Ru, H. Q. & Xiong, Y. 2016 The recovery of molybdenum(VI) from rhenium(VII) on amino-functionalized mesoporous materials. *Hydrometallurgy* **165**, 251–260.

Sun, Y. M., Hu, X. L., Luo, W. & Huang, Y. H. 2011 Self-assembled hierarchical MoO_2/graphene nanoarchitectures and their application as a high-performance anode material for lithium-ion batteries. *ASC Nano* **5** (9), 7100–7107.

Tu, Y. J., You, C. F., Chang, C. K., Chan, T. S. & Li, S. H. 2014 XANES evidence of molybdenum adsorption onto novel fabricated nano-magnetic $CuFe_2O_4$. *Chemical Engineering Journal* **244** (10), 343–349.

Tu, Y. J., Chan, T. S., Tu, H. W., Wang, S. L., You, C. F. & Chang, C. K. 2016 Rapid and efficient removal/recovery of molybdenum onto $ZnFe_2O_4$ nanoparticles. *Chemosphere* **148**, 452–458.

Xiong, Y., Chen, C. B., Gu, X. J., Biswas, B. K., Shan, W. J., Lou, Z. N., Fang, D. W. & Zang, S. L. 2011 Investigation on the removal of Mo(VI) from Mo-Re containing wastewater by chemically modified persimmon residua. *Bioresource Technology* **102** (13), 6857–6862.

Yao, Y., Gao, B., Wu, F., Zhang, C. Z. & Yang, L. Y. 2015 Engineered biochar from biofuel residue: characterization and its silver removal potential. *ACS Applied Materials & Interfaces* **7**, 10634–10640.

Yavuz, E., Özdokur, K. V., Çakar, I., Koçak, S. & Ertaş, F. N. 2015 Electrochemical preparation, characterization of molybdenum-oxide/platinum binary catalysts and its application to oxygen reduction reaction in weakly acidic medium. *Electrochimica Acta* **151**, 72–80.

First received 14 November 2017; accepted in revised form 30 May 2018. Available online 11 June 2018